

Quality Assessment of Printable Strain Hardening Cementitious Composites Manufactured in Two Different Printing Facilities

Figueiredo, Stefan C.; Overmeir, Anne L. van; Nefs, Karsten; Schlangen, Erik; Salet, Theo A. M.; Šavija, Branko; Suiker, Akke S. J.; Bos, Freek P.

DOI

[10.1007/978-3-030-49916-7_81](https://doi.org/10.1007/978-3-030-49916-7_81)

Publication date

2020

Document Version

Final published version

Published in

Second RILEM International Conference on Concrete and Digital Fabrication

Citation (APA)

Figueiredo, S. C., Overmeir, A. L. V., Nefs, K., Schlangen, E., Salet, T. A. M., Šavija, B., Suiker, A. S. J., & Bos, F. P. (2020). Quality Assessment of Printable Strain Hardening Cementitious Composites Manufactured in Two Different Printing Facilities. In F. P. Bos, S. S. Lucas, R. J. M. Wolfs, & T. A. M. Salet (Eds.), *Second RILEM International Conference on Concrete and Digital Fabrication* (pp. 824-838). (RILEM Bookseries; Vol. 28). Springer. https://doi.org/10.1007/978-3-030-49916-7_81

Important note

To cite this publication, please use the final published version (if applicable).
Please check the document version above.

Copyright

Other than for strictly personal use, it is not permitted to download, forward or distribute the text or part of it, without the consent of the author(s) and/or copyright holder(s), unless the work is under an open content license such as Creative Commons.

Takedown policy

Please contact us and provide details if you believe this document breaches copyrights.
We will remove access to the work immediately and investigate your claim.

Green Open Access added to TU Delft Institutional Repository

'You share, we take care!' – Taverne project

<https://www.openaccess.nl/en/you-share-we-take-care>

Otherwise as indicated in the copyright section: the publisher is the copyright holder of this work and the author uses the Dutch legislation to make this work public.



Quality Assessment of Printable Strain Hardening Cementitious Composites Manufactured in Two Different Printing Facilities

Stefan C. Figueiredo¹(✉), Anne L. van Overmeir², Karsten Nefs¹, Erik Schlangen², Theo A.M. Salet¹, Branko Šavija², Akke S. J. Suiker¹, and Freek P. Bos¹

¹ Eindhoven University of Technology, Eindhoven, Netherlands
s.chaves.figueiredo@tue.nl

² Delft University of Technology, Delft, Netherlands

Abstract. Over the past few years, several studies have shown the potential of three-dimensional concrete printing (3DCP) for applications in building and civil engineering. However, only a few studies have compared the properties of the fresh printing material and the quality of the printed elements from different printing facilities. Variations in the manufacturing conditions caused by the mixing procedures, the pumping device and the nozzle shape and/or dimensions may influence the quality of the printed elements. This study investigates the differences in the fresh and hardened properties of a printing material tested in two different printing facilities. The pump pressure and temperature experienced by the printing material during the printing session are monitored real-time. Hardened properties are measured for the printed elements, such as the bending capacity, the apparent density, and the air void content. The research shows that two different printing facilities may result in printed elements with relative differences in flexural strength and volumetric density of 49% and 7%, respectively.

Keywords: SHCC · ECC · Quality control · 3D concrete printing

1 Introduction

Three-dimensional concrete printing (3DCP) is one of the additive manufacturing (AM) methods currently under development for applications in the building industry. Over the last decade, extensive research has been conducted on this new technology, as it has the potential to lead to significant economic benefits by speeding up the production process, and by reducing the formwork costs. It also offers promising environmental advantages, e.g., by minimizing the use of material through the application of structural shape optimization. Moreover, benefits have been identified in regard to the increase in freedom of

design and the decrease of hard physical labour [1–3]. Current research focuses, among others, on the printing process, on the development of suitable concrete mix designs, and on the fresh and hardened material properties of the printed concrete. Collaborative projects between universities and industry have already resulted into several printed concrete structures being applied in practice, such as 3D printed concrete bridges [4].

One of the challenges within the development of 3DCP is the improvement of the limited ductility of printed mortars. Traditionally, steel rebars are used to transfer tensile stresses in concrete and to increase the ductility during fracture, in accordance with building regulations on structural integrity and safety. However, for 3D printed concrete the incorporation of traditional steel rebar reinforcement is not straightforward [5, 6], as a result of which several alternative solutions have been considered. Firstly, the application of passive reinforcement steel has been suggested, for example, by using reinforcement meshes [7], by connecting the printed concrete element to an external steel reinforcement framework [8], or through the application of an advanced printing nozzle that lays down a steel wire within the concrete layer during its printing [9, 10]. Secondly, post-tensioned, pre-stressed reinforcement may be applied. In this method, the concrete elements are printed without reinforcement; instead, the reinforcement is placed in the slots of the printed elements after assembly, and is subsequently pre-stressed in accordance with design specifications [4, 11].

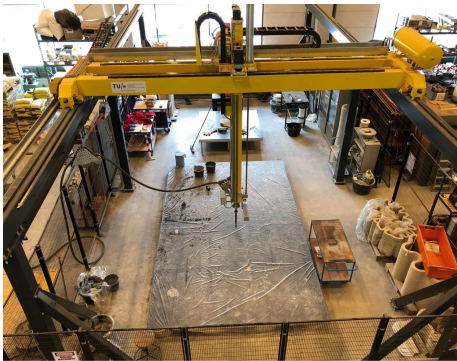
Another option of reinforcing fresh concrete in 3D printing processes is through the application of fibre-reinforced cementitious composites. A promising printing material that is characterized by both a high ductility and a high tensile strength is a strain hardening cementitious composite (SHCC). The mechanical performance of such composites is achieved by a tailored bond interface between the matrix and the fibre. Accordingly, the fibres are able to bridge a microcrack and transfer the tensile load that created the crack. Due to this bridging effect, the actual microcrack remains stable and does not grow into a macrocrack upon a further increase in loading. Instead, the stress is redistributed, which may induce a microcrack elsewhere in the concrete element that subsequently is also bridged by the fibre reinforcement. This repetition of the formation and bridging of microcracks effectively results in a strain hardening behaviour of the concrete element [12]. Since SHCCs are characterized by a relatively high tensile strength and a reliable ductility, it's worth to consider them a candidate for 3D concrete printing. Indeed, several studies have recently demonstrated the potential of this composite in 3D printing applications [13–16].

Preliminary research conducted at the Delft University of Technology and Eindhoven University of Technology has indicated that the printing settings utilized may have a significant influence on the final mechanical characteristics of the printed element. For example, relative differences up to 29% were found for the compressive strength obtained from specimens printed with the same mixture [6, 14]. Since the mechanical performance of the SHCC strongly depends on an optimal balance of the matrix and fibre properties, small deviations in the printing process may have a substantial influence on the effective mechanical behaviour of the composite. This research investigates the influence of the

printing facility on the mechanical properties of hardened SHCC specimens manufactured by 3D printing. Accordingly, printing sessions were conducted with two different printing facilities, one located at the Delft University of Technology and one located at the Eindhoven University of Technology. The mix design, mixing procedure and printing routine were kept the same, and the temperature and pumping pressure were monitored during the printing session. After hardening, the printed elements were subjected to a three-point bending test with crack mouth opening control in order to characterize the fracture response and determine the fracture properties. Further, the apparent density was measured and the air void content was analysed.

2 Printing Facilities

The printing facilities at the technical universities of Eindhoven and Delft use a gantry system for creating the contour of the printed elements. The gantry systems in Eindhoven and Delft are illustrated in Fig. 1, and are able to print volumes of $[9 \times 4.5 \times 2.8] \text{ m}^3$ and $[1 \times 0.6 \times 0.35] \text{ m}^3$, respectively. The printing facilities are equipped with a mixing device and a pump, which are connected to a 5 m hose provided with a down flow nozzle. The hose has a diameter of 25 mm, and the nozzle has a rectangular cross-section of $[40 \times 14] \text{ mm}^2$.



(a) Eindhoven $[9 \times 4.5 \times 2.8] \text{ m}^3$



(b) Delft $[1 \times 0.6 \times 0.35] \text{ m}^3$

Fig. 1. Gantry system used in both printing facilities.

The mixing devices are both of the planetary type, but differ in volume capacity, engine power and operating speed. The mixing device in Eindhoven uses a TMV 75 pan mixer fabricated by Van der Zalm Nuth B.V., and is characterized by a capacity of 75 litres, an engine power of 2.2 kW, and a single rotational speed. In Delft, an A120N Hobart pan mixer is used, characterized by a volume capacity of 12 litres, an engine power of 0.27 kW, and three rotational speeds. Figures 2(a) and 2(b) illustrate the mixers used in both facilities. Due to the different specifications

of the engine power and printing volume, the mixing procedure in Delft was carried out in 7 batches of 3 litres each, while in Eindhoven a total volume of 28 litres was mixed in one batch. The pumps used in Eindhoven and Delft are an M-tec duo-mix connect and a PFT Swing L, respectively. The main differences between these pumps relate to the design of the rotor/stator and the mixing paddles that collect the material from the reservoir and push it through the rotor/stator. The pump components are illustrated in Figs. 2(c)–2(f).

3 Methodology

3.1 Materials and Specimen Preparation

The mix design used in the research has been developed recently Delft University of Technology, see [14] for more details. The specific composition can be found in Table 1.

Table 1. Mix proportion [kg/m³]

Raw materials	XVA3PVA20
CEM I 42.5	259.2
Blast furnace slag	604.9
Limestone powder	894.1
PVA fibres (Kuraray REC15)	26
Viscosity modifier admixture (VMA)	5.1
Superplasticizer	17.3
Water	345.6

The mixing procedure adopted in Delft was as follows:

- All dry materials were mixed for two minutes at a relatively low rotational speed of 60 rpm.
- During approximately one minute, water mixed with a superplasticizer was added.
- Next, the wet powders were mixed for two minutes, whereby a significant change in the mixture’s viscosity was observed.
- The dough-like mixture was further mixed for four minutes at a moderate rotational speed of 124 rpm.

The same mixing procedure was adopted in Eindhoven. However, due to the larger material volume and the use of a single rotational speed in the mixing device, the mixing time after the inclusion of the liquid ingredients was taken somewhat longer in order to achieve the same mix consistency as in Delft.

Initially, a single layer filament was printed at different speeds and constant pumping pressure, whereby the width of the filaments was measured to select



(a) Mixer in Eindhoven.



(b) Mixer in Delft.



(c) Pump paddles in Eindhoven



(d) Pump paddles in Delft



(e) Rotor/stator in Eindhoven



(f) Rotor/stator in Delft

Fig. 2. Comparison of the components of the printing facilities used at the Technical Universities of Eindhoven and Delft.

the optimal printing speed. Subsequently, two to three objects were printed with a height of five layers. The objects were kept on the printing table for 24 h, after which they were cured in water for 13 days. Subsequently, specimens of $[40 \times 40 \times 160] \text{ mm}^3$ were sawn from the hardened object, see Fig. 3, which were subjected to mechanical testing the next day (day 14).

3.2 Fresh State

During the printing session, the pressure in the hose and the temperature of the printing material were monitored continuously. Pressure drops may indicate potential failures in the extruded material due to the development of large air pockets, and temperature changes in the printing material may lead to significant alterations in its rheological properties and hydration speed. The pumping pressure was measured by installing analogical manometers directly behind the pump and just before the printing nozzle. The pressure measured by the sensors was recorded and the values were read off after completing the printing of the object. The heat development was monitored by means of two thermocouples installed on the manometers. Accordingly, the temperature reached in the printing facilities could be determined, and the origin of the heat generated during the pumping process could be identified.

3.3 Fracture Behaviour

The fracture behaviour of the hardened specimens was determined by means of a Crack Mouth Opening Displacement (CMOD) test: a 3-point bending test on notched beams in which the load point displacement is controlled by the gradually increasing opening of the notch, known as the CMOD value. All the tests were performed on an Instron universal test rig of the Eindhoven University of Technology. Initially at a crack mouth opening rate of 0.05 mm/min until an opening of 0.1 mm was reached. The test was continued at 0.10 mm/min of CMOD until the opening reached 2.6 mm at which point the test was discontinued. The applied CMOD experiment is a scaled down version of the test detailed in EN 14651 [17], to the size of beams used for the characterization of cementitious mortars ([i.e. $40 \times 40 \times 160] \text{ mm}^3$, cf. EN 196 [18]). This corresponds to a scale factor of approximately 0.27 and results in specimen dimensions that are more appropriate in the context of 3DCP. The bending test span was 130 mm. A 3 mm wide, 7 mm (± 0.5 mm) deep notch was sawn into each specimen, leaving an effective section height at the notch of $h_{sp} = 33$ mm. More extensive descriptions and a discussion on a potential size effect of this scaled-down CMOD test are provided in [19].

Specimens were sawn with an accuracy of ± 2 mm from rectangular objects printed in Eindhoven ('E') and Delft ('D'). The specimen length corresponded with the filament printing direction, indicated as direction I. Figure 3 and Table 2 provide an overview of printed objects, obtained specimens and direction definitions. In the majority of specimens, the notch was applied across the filament width, in direction II. These specimens were labelled $I\alpha$. In some additional

D-specimens the notch was applied in direction III to study potential directional effects associated with the subsequent 90° rotation of the specimen during testing. These were named $I\beta$.

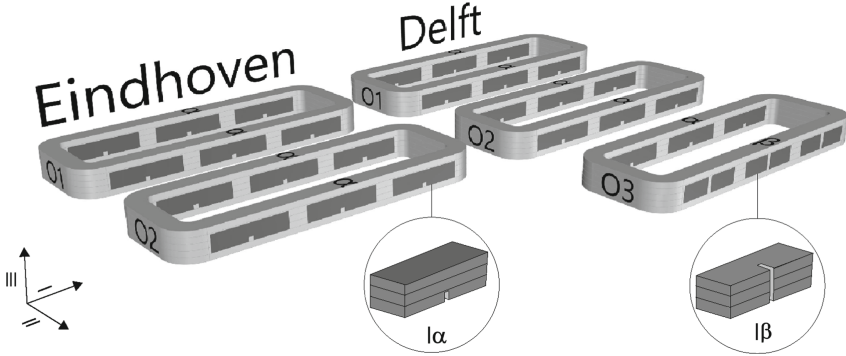


Fig. 3. Printed objects in Delft and Eindhoven with indicated specimen orientations $I\alpha$ and $I\beta$.

Table 2. Number of CMOD experiments and specimen orientations of the test programs performed.

	Eindhoven	Delft
Printed object 1 (O1)	6× CMOD-E- $I\alpha$	6× CMOD-D- $I\alpha$
Printed object 2 (O2)	6× CMOD-E- $I\alpha$	6× CMOD-D- $I\alpha$
Printed object 3 (O3)		3× CMOD-D- $I\alpha$, 3x CMOD-D- $I\beta$

3.4 Apparent Density and Air Void Content

The apparent density of the hardened specimens was assessed by measuring their weight and volume after the CMOD test. Based on the apparent density of the SHCC, the printing quality can be estimated. Additionally, a single core of 13.6 mm diameter was drilled from one object printed by the facilities in Delft and Eindhoven. This core was subjected to a micro-computed tomography scanning procedure (μ CT-scan). An acceleration voltage of 130 kV and beam current of $220 \mu\text{A}$ were applied. The pictures obtained from the scans were created from an average of two radiographs with an exposure time of 0.5 s, each generating a total of 1441 pictures. In this way, pictures with a resolution of $8.33 \mu\text{m}/\text{pixel}$ were obtained.

The software phoenix datos | $\times 2.0$ was used for reconstructing the three-dimensional specimen volume. The software centralizes the radiographs generated during the scan. Additionally, a beam hardening correction of 8 was used to correct for artefacts. With the help of the software VGStudio MAX 2.0, the image stack from the top and the right side view were obtained from the three-dimensional specimen volume and a median filter of 3 pixels in all directions was applied to the images. For analyzing the air void content and distribution in the image stack, the software ImageJ was employed. A grey value threshold was imposed in order to distinguish and isolate the air voids from the original images. In the new images of the void distribution, the size and content of the air voids with an area bigger than 40 pixel² and a circularity between 0.3 and 1.0 were counted. These filter values were applied to minimize the effect of the voids surrounding the fibres.

4 Results and Discussion

4.1 Assessment of the 3D Printing Process

The variation in temperature and pump pressure, as measured during the sequential printing of all objects, is summarized in Figs. 4(a) and 4(b) for the 3D printing facilities in Eindhoven and Delft, respectively. The pressure values obtained from the manometers installed close to the nozzle turned out to be very low, and therefore could not be read with sufficient accuracy. The pump pressure measured in the Eindhoven 3D printing facility on average is smaller than the pump pressure measured in the Delft 3D printing facility. Such pressure differences may be ascribed to various effects, such as differences in temperature, air void content, and alterations in static pressure height caused by moving the hose during the 3D printing process. In both printing facilities, the temperature rose from the moment the printing process started, whereby after some time a constant, stable temperature was reached.

In Eindhoven, the measuring of the pump pressure started from the very beginning of the 3D printing process, i.e., as soon as the material was pumped through the system, while in Delft the measuring started after the printing of 1.5 layers. This explains why the initial temperatures measured at the nozzle and in the pump are slightly different in Figs. 4(a) and 4(b). Observe further that the temperature of the printing material used in Eindhoven went up to 35°C, while in Delft the maximal temperature was approximately 27°C. This rise in temperature is believed to be due to frictional effects between the rotor and the inner part of the stator. Moreover, the observed difference in temperature rise between the two printing facilities can originate from the geometries of the rotor/stator, as has been illustrated in Figs. 2(e) and 2(f). It can be further observed that the temperature at the pump is higher than at the nozzle, which is due to heat being dissipated during material transport through the hose. In general, a printing material used in relatively long printing sessions is clearly exposed to a significant temperature increase, which will change its rheological

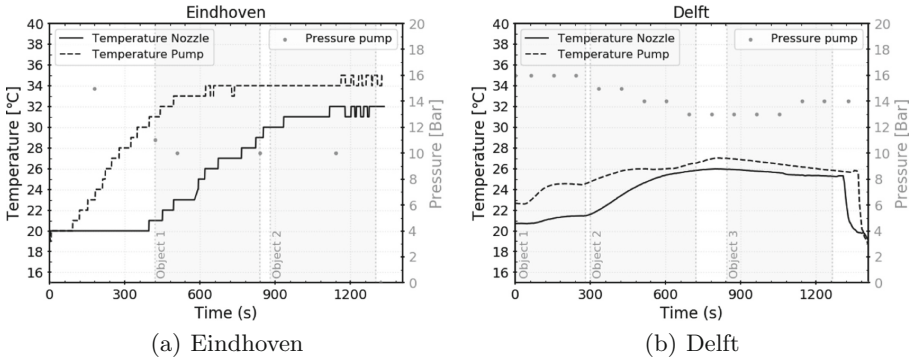


Fig. 4. Temperature and pressure profiles measured during the sequential printing of the objects.

properties, such as the buildability, see [20] for more details on this aspect. It is also noted that a temperature increase of the fresh printing material can accelerate water evaporation, which eventually might cause cracking due to shrinkage.

4.2 Failure Response in CMOD Test

The obtained flexural strength vs CMOD value curves are presented in Fig. 5. On the horizontal CMOD axis, the values of 0.135 mm, 0.405 mm, 0.675 mm, and 0.945 mm have been indicated, corresponding to 0.27 times the so-called CMOD₁ to CMOD₄ values as predefined by the EN 14651 [17]. Table 3 lists the average values of the (residual) strength parameters derived from the CMOD test: f_{LOP} is the Limit of Proportionality as defined by [18]; f_t is the maximum flexural strength; $f_{R,1} * 0.27$ and $f_{R,3} * 0.27$ are the residual strengths at the predefined CMOD values CMOD₁ and CMOD₃, respectively. In addition, the classification according to the fib Model Code 2010 [21] to characterize the residual strength is given, which is determined by the ratio of $f_{R,3} * 0.27 / f_{R,1} * 0.27$ (also provided in the table).

Figures 5(a) and 5(b) depict the results of the specimens sawn from the first object printed in Eindhoven and Delft, respectively. It can be seen that, after the initial stiff response that lasts until crack initiation, the load increases to a maximum that is reached at some point between the CMOD₁ and CMOD₄ values (i.e. strain-hardening), depending on the individual specimen. After reaching the maximum strength, the flexural stress gradually drops with deformation, showing a rather ductile softening response. The failure behaviour can clearly be ascribed to the bridging of the cracks by the fibres. Remarkably, the average maximum flexural strength f_t of the Delft specimens is 38.4% higher than that of the Eindhoven specimens. For the specimens sawn from the second object printed, this difference is even larger, namely 51.4%, see Figs. 5(c) and 5(d). The residual strength classification of the Delft specimens is also slightly better,

ranging from 'd' to 'e', while the Eindhoven specimens vary from 'c' to 'e' (details on this classification can be found in [21]).

Table 3. Average results of the CMOD tests.

	f_t [MPa]	f_{LOP} [MPa]	$f_{R,1} * 0.27$ [MPa]	$f_{R,3} * 0.27$ [MPa]	$f_{R,3} * 0.27 /$ $f_{R,1} * 0.27$	Class
CMOD-E-I α -O1	5.29	3.52	4.06	4.59	1.13	c-e
CMOD-E-I α -O2	4.99	3.14	3.87	4.83	1.25	d-e
CMOD-D-I α -O1	7.32	4.03	5.03	6.92	1.39	d-e
CMOD-D-I α -O2	7.56	4.41	5.48	7.27	1.33	d-e
CMOD-D-I α -O3	7.76	3.92	4.99	7.27	1.46	e
CMOD-D-I β -O3	8.17	4.46	5.49	7.92	1.44	e

When comparing specimens sawn from different objects printed at the same 3D printing facility, the differences in maximum flexural strength are not substantial. As can be observed in Fig. 6, the relative difference in strength of specimens from the first and second objects printed is 5.6% (Eindhoven) and 3.3% (Delft), and 5.9% (Delft) for specimens from the first and third object printed. Also, the notch orientation (and associated specimen orientation during testing) did not significantly influence the failure response. The significant differences in the flexural strength of the specimens printed in Eindhoven and Delft may be associated with differences in the internal material structure, which will be analyzed in more detail in the section below.

4.3 Apparent Density and Air Void Content

After the CMOD experiments were performed, the apparent density of the specimens was measured. The results summarized in Fig. 6 show that the average apparent densities, plotted by the light (Eindhoven) and dark (Delft) grey bars, did not change significantly during the printing sessions. Further, the specimens manufactured in Delft have an average density that is approximately 7% higher than those manufactured in Eindhoven, which explains their higher flexural strength indicated by the oblique hatched bars.

The cross-sectional images obtained from the μ CT-scan of the specimen indicate a significant variation in air void content within the layers, see Figs. 7 and 8. Moreover, the distribution of the air void sizes across the specimen height shows that the interfaces between printed layers show a local increase in air void size. For the Delft specimen the average air void content within the layers ranges from 6.7% to 8%, while for the Eindhoven specimen it ranges from 15.2 up to 19.7%. This explains why the density and flexural strength of the Delft specimens are higher than those of the Eindhoven specimens. Further, the layer interfaces of the Delft specimen shows to have a higher average air void content than within the layers, while the Eindhoven specimen show the opposite trend.

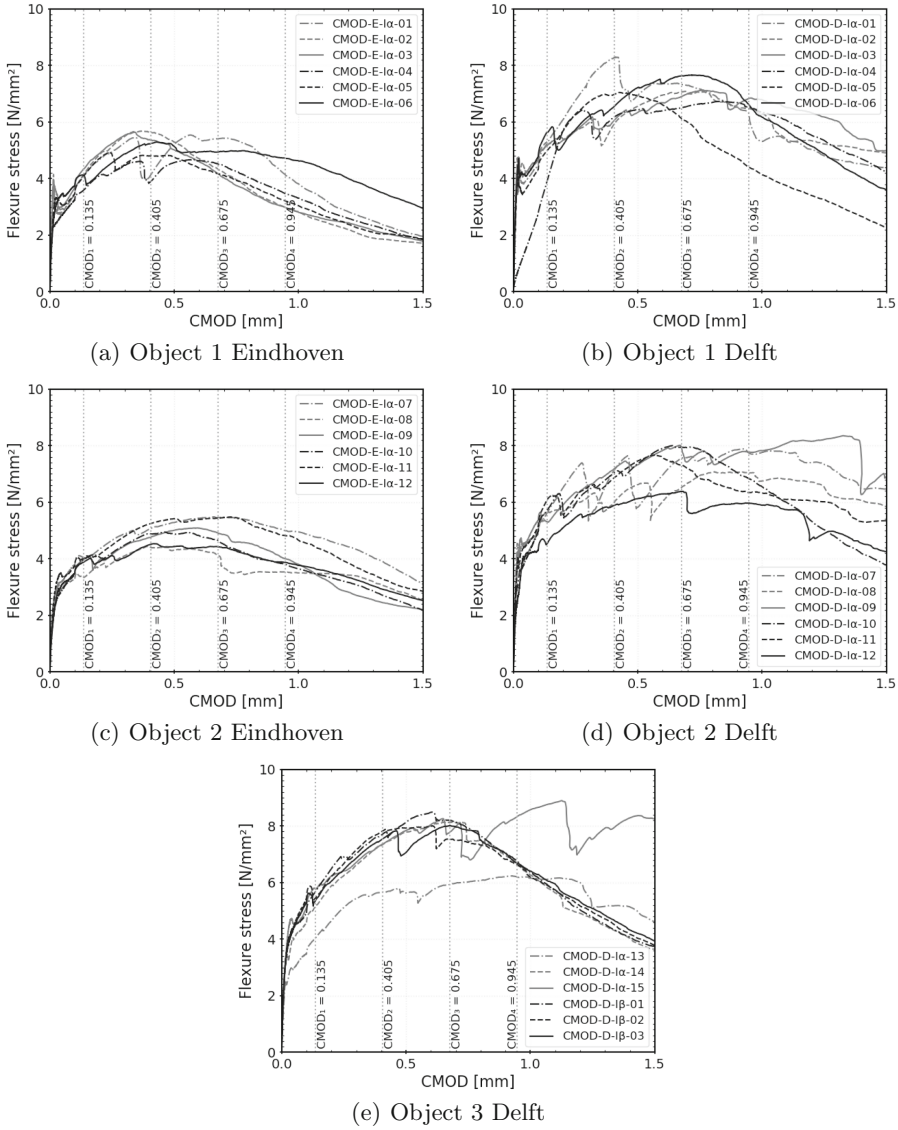


Fig. 5. Flexural stress versus CMOD of all specimens.

In addition, for both the Delft and Eindhoven specimens the void size within the layers is in the range of 0.01 to 0.016 pixel². However, for the Delft specimen the voids at the layer interface range from 0.016–0.031 pixel², which is larger than the range of 0.016 to 0.026 pixel² measured for the Eindhoven specimen. Hence, the layers interfaces of the objects printed in the Delft facility contain larger air voids than the layer interfaces of the objects printed in Eindhoven.

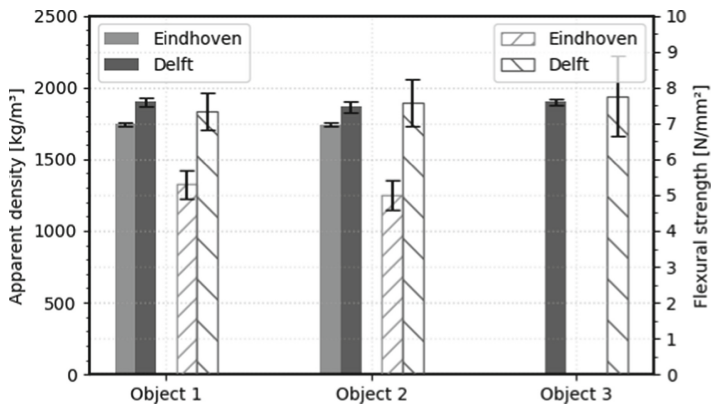


Fig. 6. Average apparent density (grey) and average flexural strength (hatched) of the specimens manufactured in Delft and Eindhoven.

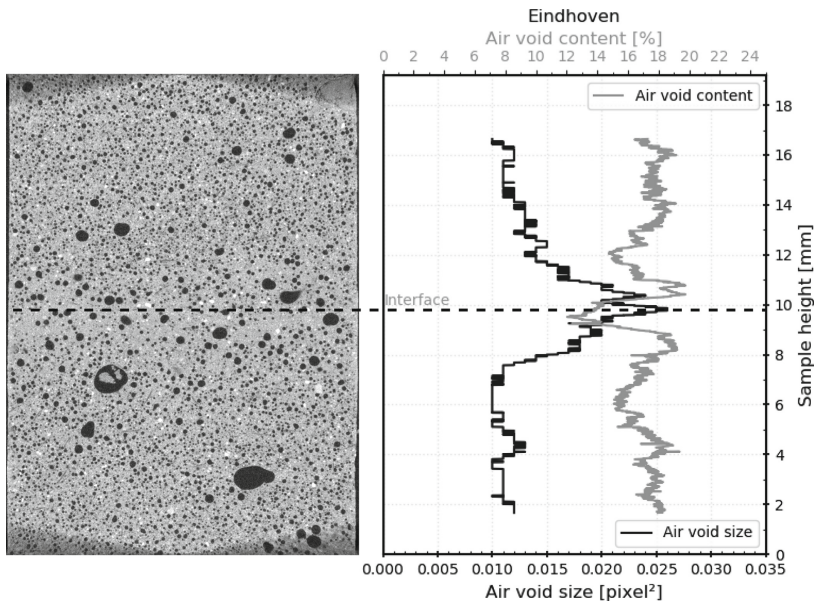


Fig. 7. Air void content and size across the height of a specimen printed in Eindhoven. The dashed line designates the interface between the printed layers.

Figure 9 shows an example of relatively large air voids found within the printed layers in a Delft specimen.

The differences in the properties observed for hardened specimens may originate from the mixing characteristics of the fresh concrete, such as the dissolution time from the VMA or superplasticizer, the fibre dispersion, and the entrapment

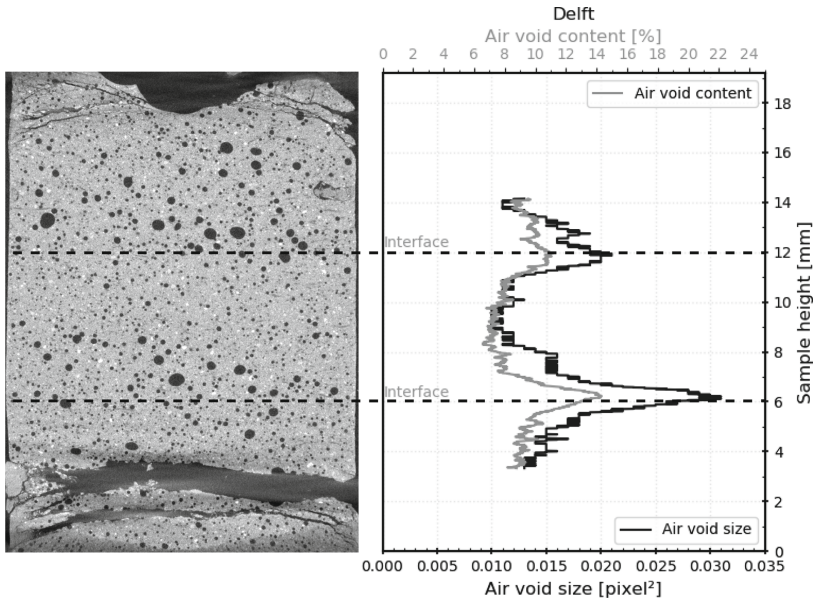


Fig. 8. Air void content and size across the height of a specimen printed in Delft. The dashed line designates the interface between the printed layers.

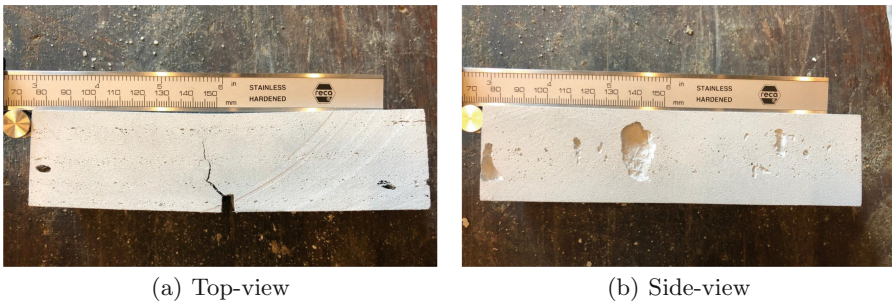


Fig. 9. Large air voids in specimen printed in Delft and tested in direction $I\alpha$.

of air during mixing. Previous work has indeed demonstrated how VMA can influence the total air void content of the cement paste [22]. Additionally, it is important to emphasize that the mixer in Eindhoven is significantly more powerful than the one in Delft, and that the mixing time in Eindhoven was adapted to reach the same visible consistency. Therefore, it may be reasonably expected that the mixing procedure has a strong effect on the total air void content of the printed material.

The relatively large air voids found in specimens from Delft could be explained by the pumping mechanism. The paddles, exemplified in Figs. 2(c)

and 2(d), rotate in order to collect the material from the reservoir and push it towards the rotor/stator. Due to the high viscosity of printable SHCCs, some air pockets might have been created during this stage. It is hypothesised that a coarse rotor/stator system (Delft) can transport these large air pockets as a whole, whereas a fine rotor/stator system (Eindhoven) might break these large air voids down into smaller voids. However, more research is needed to explore such differences in more detail.

5 Conclusions

- The mechanical and physical properties of the specimens manufactured in the 3D printing facilities in Delft and Eindhoven were significantly different. In order to reduce these differences, standardization of printing methods and full understanding of printing variables is of crucial importance.
- The mixing time and intensity have a strong influence on the quality of dough-like mixtures. Longer mixing times introduce entrapment of air voids in the fresh state, which causes a reduction in mechanical properties.
- Based on the collected data no significant differences were found in the mechanical results in relation to the temperature history of each object.
- The total air content found in specimens mixed and printed at different 3D printing facilities may vary significantly. This turns out to have a considerable effect on the mechanical properties in the hardened state.

Acknowledgements. This research was funded through the NWO Open Technology Program, project ‘High Performance 3D Concrete Printing’, grant number 17251.

References

1. Wangler, T., Lloret, E., Reiter, L., Hack, N., Gramazio, F., Kohler, M., Bernhard, M., Dillenburger, B., Buchli, J., Roussel, N., Flatt, R.: Digital concrete: opportunities and challenges. *RILEM Tech. Lett.* **1**, 67–75 (2016)
2. Buswell, R., de Silva, W.L., Jones, S., Dirrenberger, J.: 3D printing using concrete extrusion: a roadmap for research. *Cem. Concr. Res.* **112**, 37–49 (2018). SI: Digital concrete 2018
3. Asprone, D., Menna, C., Bos, F.P., Salet, T.A., Mata-Falcón, J., Kaufmann, W.: Rethinking reinforcement for digital fabrication with concrete. *Cem. Concr. Res.* **112**, 111–121 (2018). SI: Digital concrete 2018
4. Salet, T.A.M., Ahmed, Z.Y., Bos, F.P., Laagland, H.L.M.: Design of a 3D printed concrete bridge by testing. *Virtual Phys. Prototyping* **13**(3), 222–236 (2018)
5. Bos, F., Wolfs, R., Ahmed, Z., Salet, T.: Additive manufacturing of concrete in construction: potentials and challenges of 3D concrete printing. *Virtual Phys. Prototyping* **11**(3), 209–225 (2016)
6. Van Overmeir, A.L.: Designing an interlayer reinforcement solution for printable strain-hardening cement-based composites.: Practical research on various bond improvement concepts. Master’s thesis, Delft University of Technology (2020)
7. Marchment, T., Sanjayan, J.: Mesh reinforcing method for 3D concrete printing. *Autom. Constr.* **109**, 102992 (2020)

8. Asprone, D., Auricchio, F., Menna, C., Mercuri, V.: 3D printing of reinforced concrete elements: technology and design approach. *Constr. Build. Mater.* **165**, 218–231 (2018)
9. Bos, F.P., Ahmed, Z.Y., Wolfs, R.J.M., Salet, T.A.M.: 3D printing concrete with reinforcement. In: Hordijk, D., Luković, M. (eds.) *High Tech Concrete: Where Technology and Engineering Meet*, pp. 2484–2493. Springer, Cham (2018)
10. Ma, G., Li, Z., Wang, L., Bai, G.: Micro-cable reinforced geopolymer composite for extrusion-based 3D printing. *Mater. Lett.* **235**, 144–147 (2019)
11. Lim, S., Buswell, R., Le, T., Wackrow, R., Austin, S., Gibb, A., Thorpe, A.: Development of a viable concrete printing process. In: *Proceedings of the 28th International Symposium on Automation and Robotics in Construction, ISARC 2011* (2011)
12. Li, V.C.: On engineered cementitious composites (ecc). *J. Adv. Concr. Technol.* **1**(3), 215–230 (2003)
13. Soltan, D.G., Li, V.C.: A self-reinforced cementitious composite for building-scale 3D printing. *Cem. Concr. Compos.* **90**, 1–13 (2018)
14. Figueiredo, S.C., Rodriguez, C.R., Ahmed, Z.Y., Bos, D., Xu, Y., Salet, T.M., Çopuroğlu, O., Schlangen, E., Bos, F.P.: An approach to develop printable strain hardening cementitious composites. *Mater. Des.* **169**, 107651 (2019)
15. Ogura, H., Nerella, V., Mechtcherine, V.: Developing and testing of strain-hardening cement-based composites (SHCC) in the context of 3D-printing. *Materials* **11**(8), 1375 (2018)
16. Zhu, B., Pan, J., Nematollahi, B., Zhou, Z., Zhang, Y., Sanjayan, J.: Development of 3D printable engineered cementitious composites with ultra-high tensile ductility for digital construction. *Mater. Des.* **181**, 108088 (2019)
17. European Committee for Standardization, EN 14651:2005+A1: 2007(E) Test method for metallic fibre concrete – measuring the flexural tensile strength (limit of proportionality (LOP), residual), CEN (2007)
18. European Committee for Standardization, EN 196-1: 2016 Methods of testing cement - Part 1: Determination of strength, CEN (2016)
19. Bos, F.P., Bosco, E., Salet, T.A.M.: Ductility of 3d printed concrete reinforced with short straight steel fibers. *Virtual Phys. Prototyping* **14**(2), 160–174 (2019)
20. Wolfs, R.J.M., Suiker, A.S.J.: Structural failure during extrusion-based 3D printing processes. *Int. J. Adv. Manuf. Technol.* **104**(1–4), 565–584 (2019)
21. International Federation for Structural Concrete: *fib Model Code for Concrete Structures 2010*. Ernst & Sohn GmbH & Co., KG (2013). ISBN 978-3-433-03061-5
22. Figueiredo, S.C., Çopuroğlu, O., Schlangen, E.: Effect of viscosity modifier admixture on portland cement paste hydration and microstructure. *Constr. Build. Mater.* **212**, 818–840 (2019)